

# SCIENTIFIC REPORTS



OPEN

## Suppressed N<sub>2</sub>O formation during NH<sub>3</sub> selective catalytic reduction using vanadium on zeolitic microporous TiO<sub>2</sub>

Received: 31 March 2015

Accepted: 06 July 2015

Published: 03 August 2015

Seung Gwan Lee<sup>1</sup>, Hyun Jeong Lee<sup>1</sup>, Inhak Song<sup>2</sup>, Seunghee Youn<sup>2</sup>, Do Heui Kim<sup>2</sup> & Sung June Cho<sup>1</sup>

Emission of N<sub>2</sub>O from mobile and off-road engine is now being currently regulated because of its high impact compared to that of CO<sub>2</sub>, thereby implying that N<sub>2</sub>O formation from the exhaust gas after-treatment system should be suppressed. Selective catalytic reduction using vanadium supported TiO<sub>2</sub> catalyst in mobile and off-road engine has been considered to be major source for N<sub>2</sub>O emission in the system. Here we have demonstrated that vanadium catalyst supported on zeolitic microporous TiO<sub>2</sub> obtained from the hydrothermal reaction of bulk TiO<sub>2</sub> at 400 K in the presence of LiOH suppresses significantly the N<sub>2</sub>O emission compared to conventional VO<sub>x</sub>/TiO<sub>2</sub> catalyst, while maintaining the excellent NO<sub>x</sub> reduction, which was ascribed to the location of VO<sub>x</sub> domain in the micropore of TiO<sub>2</sub>, resulting in the strong metal support interaction. The use of zeolitic microporous TiO<sub>2</sub> provides a new way of preparing SCR catalyst with a high thermal stability and superior catalytic performance. It can be also extended further to the other catalytic system employing TiO<sub>2</sub>-based substrate.

Ever increasing demand for the reduction of greenhouse gas results in the more stringent regulation on its emission and also the corresponding research and development to capture or convert into inert molecule<sup>1</sup>. Compared to that of a major greenhouse, CO<sub>2</sub>, N<sub>2</sub>O has a high greenhouse gas effect up to 300 times<sup>2</sup>. Therefore, the impact of N<sub>2</sub>O emission can be comparable to that of CO<sub>2</sub> though the emission concentration of N<sub>2</sub>O is relatively low. Most recent diesel engine emission regulation is now started to include N<sub>2</sub>O because of its high impact and stability in stratosphere<sup>3</sup>. For diesel engine emission control under lean condition, urea SCR (selective catalytic reduction) system is *the state of art technology* for the reduction of NO<sub>x</sub> in most engine companies<sup>4</sup>. Under lean condition where the air to fuel ratio is far beyond the stoichiometric condition, the N<sub>2</sub>O formation can be suppressed readily while the system has been maintained under oxidizing condition. However, the emission of N<sub>2</sub>O from diesel engine can be increased when the reducing agent for NO<sub>x</sub> is introduced in the SCR system following the reactions, such as 2NH<sub>3</sub> + 2NO + O<sub>2</sub> = N<sub>2</sub>O + N<sub>2</sub> + 3H<sub>2</sub>O, 2NH<sub>3</sub> + 2O<sub>2</sub> = N<sub>2</sub>O + 3H<sub>2</sub>O and NH<sub>4</sub>NO<sub>3</sub> = N<sub>2</sub>O + 2H<sub>2</sub>O<sup>5</sup>. The former two reactions were believed to be the major pathway for N<sub>2</sub>O formation in which bimolecular reaction can occur.

For NO<sub>x</sub> abatement, VO<sub>x</sub> catalyst supported on TiO<sub>2</sub> has been used widely in most diesel engines<sup>5–8</sup>. There are numerous investigations on the improvement of the catalytic performance using additives such as Ce or W and also using peculiar TiO<sub>2</sub> synthesized using sol-gel method or organic or inorganic templating method<sup>9–15</sup>. However, VO<sub>x</sub> supported on TiO<sub>2</sub> of relatively low surface area is *the state of*

<sup>1</sup>Department of Applied Chemical Engineering, Chonnam National University, Yongbong 300, Buk-gu, Kwangju, 500-757, Korea. <sup>2</sup>School of Chemical and Biological Engineering, Institute of Chemical Processes, Seoul National University, 1 Gwanak-ro, Gwanak-gu, Seoul 151-744, Korea. Correspondence and requests for materials should be addressed to S.J.C. email: (sjcho@chonnam.ac.kr) or D.H.K. email: (dohkim@snu.ac.kr)

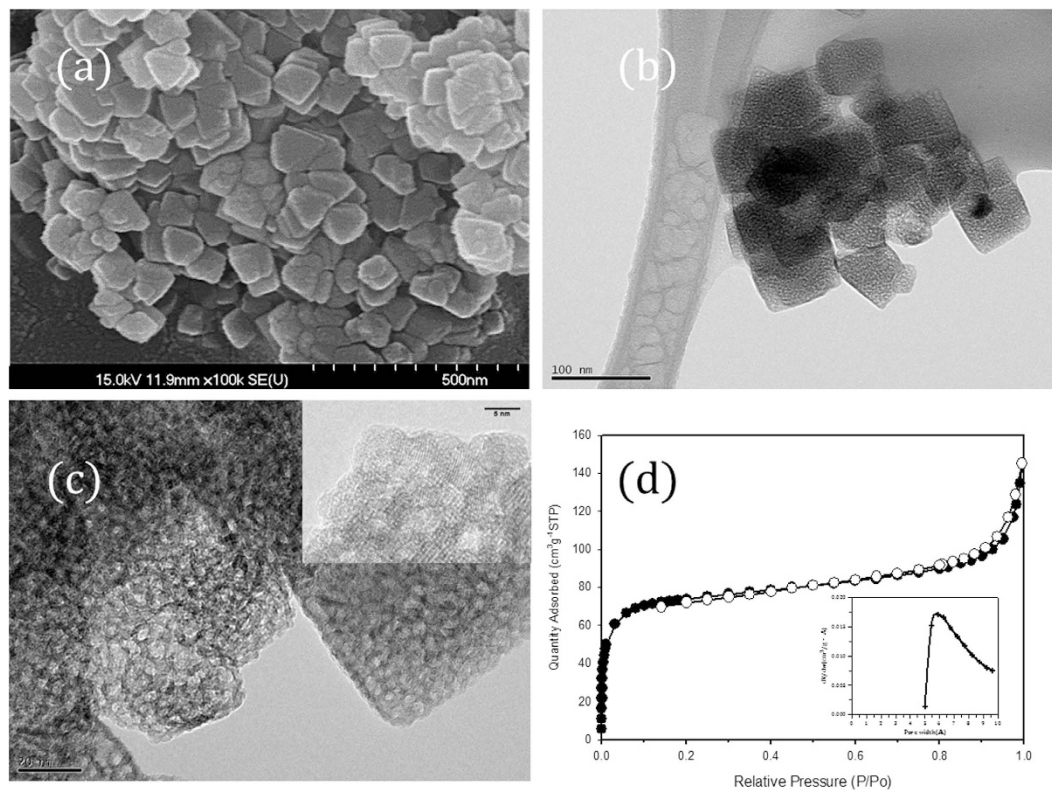


**Figure 1. Morphology of the zeolitic microporous  $\text{TiO}_2$ .** (a) Scanning electron micrographs, (b,c) transmission electron micrographs and (d) the argon adsorption-desorption isotherm of the zeolitic microporous  $\text{TiO}_2$  with the pore size distribution (inset) obtained from Horvath-Kawazoe method. The solid and open symbols indicate the adsorption and desorption branch, respectively.

*art technology* catalyst. Indeed the current  $\text{VO}_x/\text{TiO}_2$  catalyst emits  $\text{N}_2\text{O}$  when the reducing agent is present in the stream. The current emission level of  $\text{N}_2\text{O}$  is 50 mg per mile, which also depends on the catalyst composition and the system configuration such as diesel oxidation catalyst-selective catalytic reduction-diesel particulate filter<sup>3</sup>. The  $\text{N}_2\text{O}$  emission characteristics of the  $\text{VO}_x/\text{TiO}_2$  catalyst should be improved under reducing condition. For this purpose, the economically viable catalyst has to be developed in near future.

It has been demonstrated that the hydrothermal conversion of commercially available  $\text{TiO}_2$  in the presence of alkaline hydroxide produces unique  $\text{TiO}_2$  structures differently depending on the species of alkaline hydroxide<sup>16–19</sup>. Recently, the addition of  $\text{LiOH}$ ,  $\text{NaOH}$  and  $\text{KOH}$  to the hydrothermal medium was reported to be resulted in the formation of zeolitic microporous  $\text{TiO}_2$ , nanotube and nanorod, respectively<sup>19–21</sup>, which seems to be a cost effective process. The obtained microporous nanocrystalline  $\text{TiO}_2$  showed large surface area of  $250 \text{ m}^2\text{g}^{-1}$  with the pore volume of  $0.15\text{--}0.20 \text{ ccg}^{-1}$ , which was similar to those of zeolites and also suitable for catalyst preparation.

The formation mechanism of  $\text{TiO}_2$  nanotube by hydrothermal synthesis in the presence of  $\text{NaOH}$  has been studied extensively but it is not clarified yet<sup>16,22</sup>. Initial work on the formation mechanism of  $\text{TiO}_2$  nanotube suggested that the nanotube is obtained with an acid washing and subsequent  $\text{Na}^+$  ion exchange after the formation of amorphous  $\text{TiO}_2$  during hydrothermal reaction between  $\text{NaOH}$  and bulk  $\text{TiO}_2$ <sup>16,20,22–24</sup>. The other mechanism proposed that the bond breaking of 3-dimensional  $\text{TiO}_2$  structure formed layered 2-dimensional structure and finally 1-dimensional nanotubes through sheet folding mechanism<sup>22</sup>. The removal of  $\text{Na}^+$  cation from the nanotube also deteriorates readily the thermal stability when it is heated at high temperature.

However, the use of zeolitic microporous  $\text{TiO}_2$  prepared from alkaline condition has not explored yet. Thus, it is interesting to know whether the zeolitic microporous  $\text{TiO}_2$  has a high thermal stability or not and also is suitable for catalytic application as a substrate. For the first time in the present work, the zeolitic microporous nanocrystalline  $\text{TiO}_2$  has been demonstrated as a catalyst support for  $\text{VO}_x$  over selective catalytic reduction of  $\text{NO}_x$  using ammonia in order to decrease the  $\text{N}_2\text{O}$  formation.

## Results

Figure 1 shows the scanning electron micrographs and transmission electron micrographs of the zeolitic microporous  $\text{TiO}_2$  after the hydrothermal treatment. The morphology of the particle after the hydrothermal

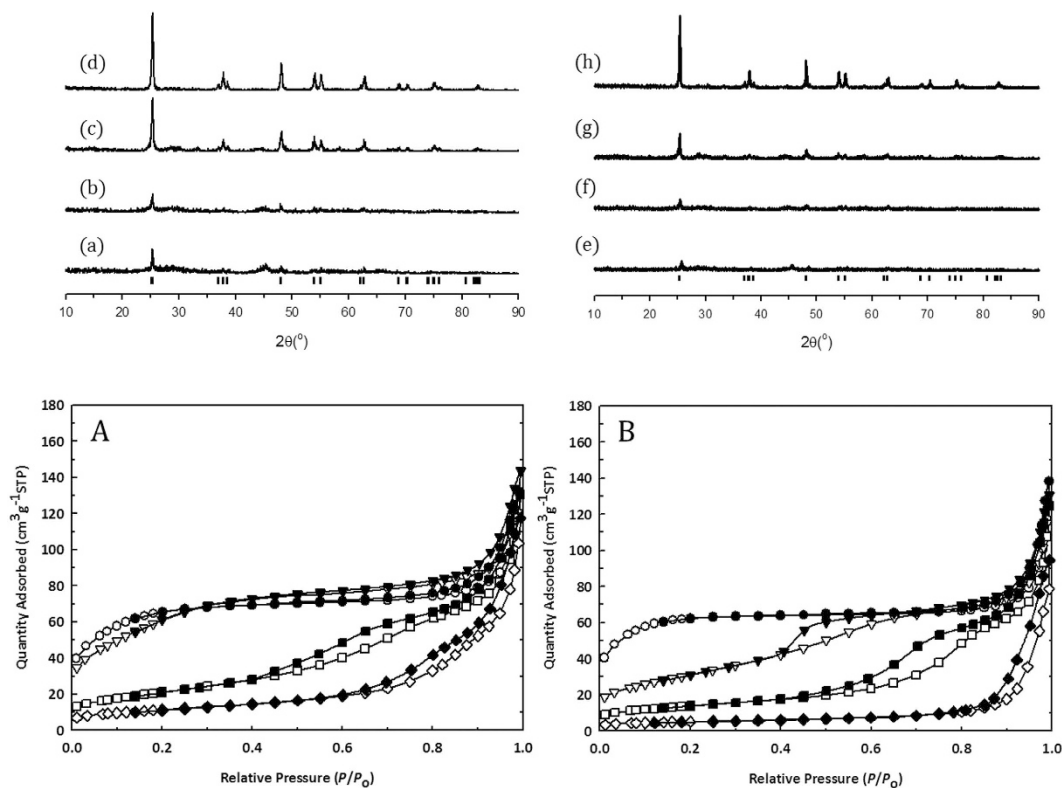


**Figure 2. Phase and surface properties of the zeolitic microporous  $\text{TiO}_2$ .** X-ray powder diffraction pattern of the zeolitic microporous  $\text{TiO}_2$  heated at (a,e) 673 K, (b,f) 773 K, (c,g) 873 K and (d,h) 973 K for 4 h, respectively, in ambient air with (upper right panel) and without saturated water (upper left panel). The tick mark corresponded to anatase phase. Nitrogen adsorption-desorption isotherm for the zeolitic microporous  $\text{TiO}_2$  heated at (○,●) 673 K, (▽,▼) 773 K, (□,■) 873 K, and (◇,◆) 973 K, respectively, in ambient air with (lower left panel, A) and without saturated water (lower right panel, B). The open and solid symbols indicate the adsorption and desorption branch, respectively.

conversion contained sharp edges, suggesting the formation of the well-crystallized  $\text{TiO}_2$ , which was consistent with the literature<sup>19–21</sup>. The obtained  $\text{TiO}_2$  had the typical argon adsorption-desorption isotherm consistent with the Langmuir isotherm type containing micropore mostly where the micropore area estimated from  $t$ -plot was  $\sim 200 \text{ m}^2 \text{ g}^{-1}$ , corresponding to 80% of the total surface area of which the pore size was estimated to be  $\sim 7 \text{ \AA}$ . The corresponding surface area and pore volume were controlled to be  $250 \pm 20 \text{ m}^2 \text{ g}^{-1}$  and  $0.20 \pm 0.05 \text{ cc g}^{-1}$ , respectively, depending on the hydrothermal reaction condition. Also, the presence of the mesopore was observed above  $P/P_0 > 0.9$  but its portion can be decreased with the increase of hydrothermal reaction time. Such mesopore formation was also shown clearly in Fig. 1(c) where the mesopore was formed with several interconnecting crystalline  $\text{TiO}_2$  frameworks of which the thickness was 3–4 nm.

Therefore, the results of the transmission electron micrograph observation supported the corresponding unique  $\text{TiO}_2$  structure containing the micropore and also the mesopore of which the size was 5–7 nm, which was consistent with the result of argon and nitrogen adsorption-desorption measurement.

The hydrothermal conversion of the bulk  $\text{TiO}_2$  into zeolitic microporous  $\text{TiO}_2$  in the presence of LiOH seems not to follow the sheet folding mechanism like  $\text{TiO}_2$  nanotube. The intercalation of  $\text{Li}^+$  ion into the  $\text{TiO}_2$  structure leads to the formation of the  $\text{Li}^+\text{-O-Ti}$  bond similar to that of  $\text{Na}^+$  case, resulting in the partial delamination of the  $\text{TiO}_2$  layer where the interaction between the layers is high enough to induce the combination of the corresponding layers<sup>25,26</sup>.

The thermal stability of the zeolitic microporous  $\text{TiO}_2$  under ambient condition either with the presence or absence of the saturated water was also investigated using the X-ray diffraction pattern (XRD) and  $\text{N}_2$  adsorption and desorption isotherms as a function of heating temperature. Nearly up to 773 K, the microporous structure was retained as evidenced from the results of the nitrogen adsorption-desorption isotherm for the sample shown in Fig. 2 even though the microporous structure was collapsed significantly with the increase of temperature in the presence of water. The XRD of the sample also showed that the crystalline anatase structure appeared to be the major phase when the samples were heated above 773 K. The combined results from XRD and nitrogen adsorption-desorption isotherm confirmed the transformation of microporous  $\text{TiO}_2$  to macroporous  $\text{TiO}_2$ . The moderate thermal stability of the zeolitic

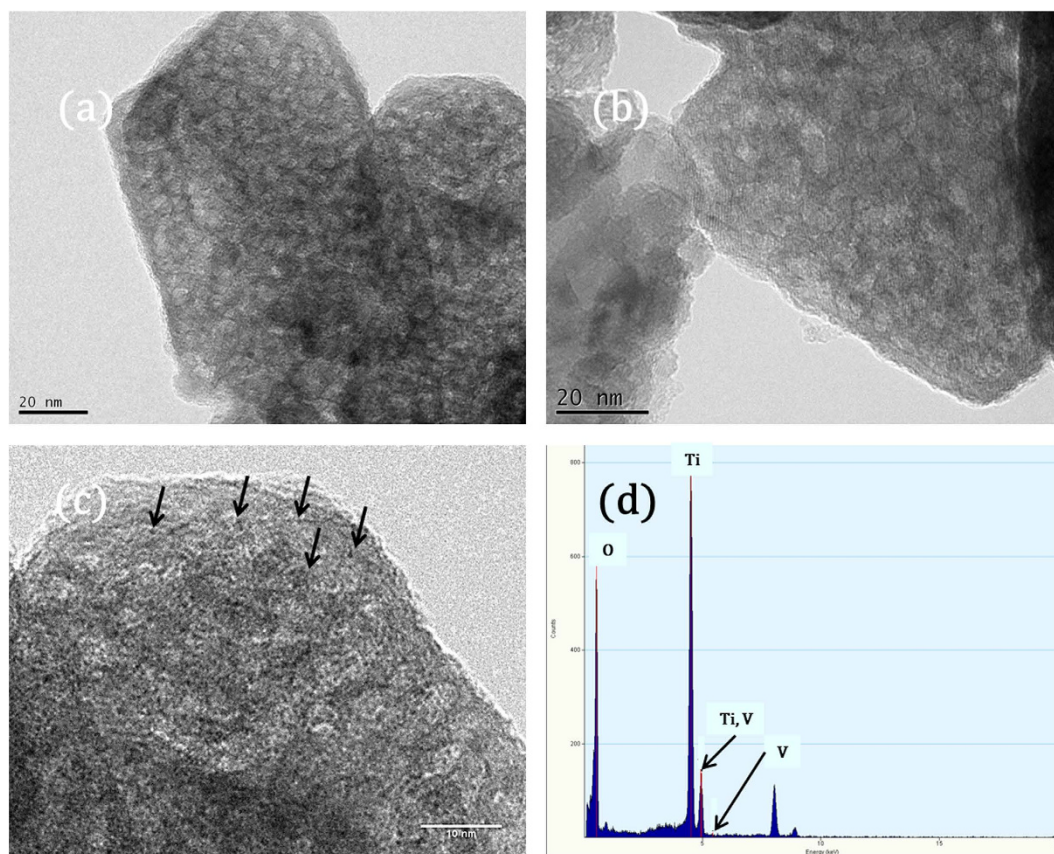


**Figure 3.** VO<sub>x</sub> encapsulated in the zeolitic microporous TiO<sub>2</sub>. Transmission electron micrographs of the microporous TiO<sub>2</sub> containing 5 wt% heated at (a,c) 673 K and (b) 773 K, respectively. The elemental analysis in (d) showed the presence of V.

microporous TiO<sub>2</sub> due to the crystal growth into anatase in the presence of water may limit the catalytic application at higher temperature. However, many catalytic applications including photocatalysis or solar energy harvesting can adopt the present zeolitic microporous TiO<sub>2</sub><sup>21</sup>.

VO<sub>x</sub> was supported onto the corresponding unique TiO<sub>2</sub> structure following the procedure reported in the literature<sup>27–32</sup>. However, the supporting VO<sub>x</sub> catalyst up to 5 wt% resulted in the lower surface area of 105 m<sup>2</sup>g<sup>-1</sup> with 0.19 ccg<sup>-1</sup> because of the high calcination temperature at 773 K though the sample still contained large surface area. These textural properties were maintained before and after the catalytic reaction measurement. The TEM observation of VO<sub>x</sub> incorporated TiO<sub>2</sub> as shown in Fig. 3 suggested that most VO<sub>x</sub> particle are located inside the pores of the zeolitic microporous TiO<sub>2</sub>, ~7 Å without changing the corresponding morphologies. Thereby, the VO<sub>x</sub> particle was observed clearly as a spot in Fig. 3(c) while there was no particle on the external surface of the TiO<sub>2</sub> though the elemental analysis showed the presence of V in the same region as shown in Fig. 3(d), which can be beneficial for the catalytic reaction. Further, increasing V content in the present also did not alter the location of V.

Figure 4 shows the catalytic performance of the V/TiO<sub>2</sub> catalyst after the calcination at different temperatures also under various reaction conditions. Increasing V content in the catalyst improved the catalytic performance of the NO<sub>x</sub> reduction comparable to that of conventional V/TiO<sub>2</sub> catalyst containing 5 wt% V over the whole reaction temperature range while the N<sub>2</sub>O formation was much lower than that of conventional catalyst. The N<sub>2</sub>O formation from the present V/TiO<sub>2</sub> was increased with the increase in the temperature where NH<sub>3</sub> was combined with NO<sub>x</sub> to produce N<sub>2</sub>O. The effect of the calcination temperature was also pronounced to increase the N<sub>2</sub>O formation at high temperature but the N<sub>2</sub>O formation was still lowered than that of the conventional catalyst by more than 80%. Also, the V/TiO<sub>2</sub> catalyst prepared from the microporous TiO<sub>2</sub> resulted in the superior catalytic performance over the SCR reaction both in the presence of water in the reactant stream and after the aging in the presence of water at 773 K for 12 h, as shown in Fig. 4(c,d). In the presence of water in the stream the low temperature catalytic activity was decreased while the high temperature catalytic activity was increased slightly because of competitive adsorption of NH<sub>3</sub> and H<sub>2</sub>O suppressing the NH<sub>3</sub> oxidation.

Under the present condition, the main reaction for N<sub>2</sub>O formation is believed to be 2NH<sub>3</sub> + 2NO + O<sub>2</sub> = N<sub>2</sub>O + N<sub>2</sub> + 3H<sub>2</sub>O following the literature<sup>3</sup>. The catalytically active VO<sub>x</sub> inside the pore, ~7 Å was believed to have a strong metal support interaction with TiO<sub>2</sub>, resulting the smaller VO<sub>x</sub> particle size

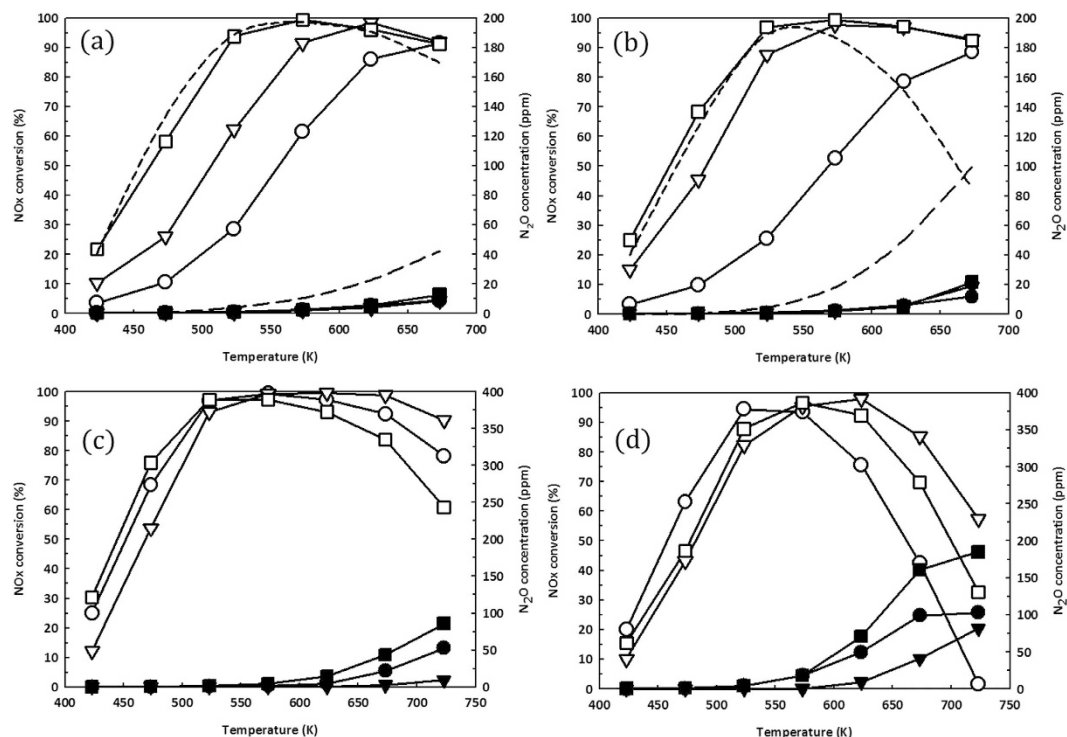


**Figure 4.** SCR activity of  $\text{VO}_x$  encapsulated in the zeolitic microporous  $\text{TiO}_2$ . Catalytic activity of  $\text{V}/\text{TiO}_2$  catalyst calcined at (a) 673 K and (b) 773 K for over  $\text{NO}_x$  reduction using ammonia: ( $\circ, \bullet$ ) 1 wt%, ( $\nabla, \blacktriangledown$ ) 3 wt% and ( $\square, \blacksquare$ ) 5 wt%. The long and short dashed lines also represent the  $\text{N}_2\text{O}$  concentration and  $\text{NO}_x$  conversion from conventional  $\text{V}/\text{TiO}_2$ , respectively. The open and solid symbols were corresponded to  $\text{NO}_x$  conversion and  $\text{N}_2\text{O}$  formation, respectively. The dashed line was the catalytic performance of commercial  $\text{V}/\text{TiO}_2$ . The reactant consisting of 500 ppm  $\text{NO}$ , 500 ppm  $\text{NH}_3$ , 2%  $\text{O}_2$  balanced with  $\text{N}_2$  was flowed through the  $\text{V}/\text{TiO}_2$  catalyst bed containing 0.15 g at  $\text{GHSV} = 40,000 \text{ h}^{-1}$ . The catalytic activity of (c) 5 wt%  $\text{V}/\text{TiO}_2$  catalyst and (d) conventional  $\text{V}/\text{TiO}_2$  catalyst calcined at 773 K were measured in the different reaction conditions: ( $\circ, \bullet$ ) dry reaction condition, ( $\nabla, \blacktriangledown$ ) wet reaction condition and ( $\square, \blacksquare$ ) dry reaction condition with hydrothermal aging at 773 K for 12 h in the presence of 5% water. In order to achieve the wet condition, the reactant consisting of 500 ppm  $\text{NO}$ , 500 ppm  $\text{NH}_3$ , 2%  $\text{O}_2$  and 3%  $\text{H}_2\text{O}$  balanced with  $\text{N}_2$  was flowed through the  $\text{V}/\text{TiO}_2$  catalyst bed at  $\text{GHSV} = 40,000 \text{ h}^{-1}$ .

as referred from Fig. 3. Thus, the strong metal-support interaction between  $\text{TiO}_2$  and  $\text{VO}_x$  led to the formation of Bronsted acid site with high strength, which is beneficial for selective catalytic reduction of  $\text{NO}$  by  $\text{NH}_3$ . The  $\text{N}_2\text{O}$  formation can be suppressed up to  $\sim 80\%$  because of the increased Bronsted acidity of the  $\text{VO}_x$  small particle in the microporous zeolitic  $\text{TiO}_2$  where the superior SCR activity can be maintained as illustrated in Fig. 4(c). This result was partly consistent with the increased  $\text{N}_2\text{O}$  formation on the  $\text{V}/\text{TiO}_2$  catalyst when the catalyst deteriorates because of the sintering<sup>3</sup>. Also, it was possible to include  $\text{NH}_3$  oxidation by  $\text{O}_2$  as potential pathway for the following  $\text{N}_2\text{O}$  formation reaction:  $2\text{NH}_3 + 2\text{O}_2 = \text{N}_2\text{O} + 3\text{H}_2\text{O}$  where the catalyst deactivation was severe like the commercial  $\text{V}/\text{TiO}_2$  catalyst in the presence of water or after hydrothermal aging. One possibility to explain the superior catalytic performance  $\text{V}$  supported on zeolitic microporous  $\text{TiO}_2$  over the SCR reaction was that the growth of the vanadium oxide particle size can be limited due to the pore size, implying the encapsulation of vanadium oxide particle surrounded by  $\text{TiO}_2$  matrix.

We have demonstrated that the zeolitic microporous  $\text{TiO}_2$  with moderate thermal stability can be prepared from the simple hydrothermal conversion from commercially available bulk  $\text{TiO}_2$  of low grade, 98% or lower in the presence of  $\text{LiOH}$  at 400–440 K, which can be scaled up easily for industrial process. The obtained zeolitic microporous nanocrystalline  $\text{TiO}_2$  contains the micropore up to 80% referred from the  $t$ -plot method. For the first time, it was proved that that the supporting  $\text{VO}_x$  into such zeolitic microporous  $\text{TiO}_2$  resulted in the high  $\text{NO}_x$  reduction activity with lower  $\text{N}_2\text{O}$  formation, which was ascribed to the location of catalytically active  $\text{VO}_x$  particles in the microporous  $\text{TiO}_2$ , resulting the strong metal-support interaction and consequently the increased Bronsted acidity. Therefore, the zeolitic microporous  $\text{TiO}_2$  has potential as a substrate for the SCR reaction below 773 K while the thermal stability of the microporous  $\text{TiO}_2$  was retained.

## Methods

**Synthesis of zeolitic microporous TiO<sub>2</sub>.** TiO<sub>2</sub> anatase (Aldrich, 98%) of 2–8 g was added to the solution containing 10 M or more LiOH in the Teflon lined autoclave for hydrothermal heating at 400–440 K for 72 hr under rotating condition at 40 rpm. After cool down to room temperature, the slurry was neutralized with 0.1 N HCl under stirring for 6 hr. The solution was filtered and washed with deionized water thoroughly. The acidification and filtration was repeated three times to remove the residual trace metal hydroxides. The obtained product was dried at 330 K in an oven and calcined under flowing oxygen at 673 K for 4 h. The inductively coupled plasma analysis of the obtained sample showed that the residual Li was ~6 ppm level, indicating the complete removal of Li<sup>+</sup> by the neutralization and subsequent thorough washing. The scale up to ~100 g per batch was also demonstrated to give the same textural properties.

**Preparation of VO<sub>x</sub> in zeolitic microporous TiO<sub>2</sub>.** All catalysts were prepared by applying wet impregnation of vanadium precursor solution on titania. Ammonium metavanadate (99%, Sigma Aldrich) was dissolved in diluted oxalic acid solution (0.5 M) to produce the solution of vanadium precursor. Anatase TiO<sub>2</sub> powder (DT-51 Millennium Chemicals) was used as support to prepare the conventional catalyst containing 5 wt% V. The samples with 1 wt%, 3 wt% and 5 wt% V<sub>2</sub>O<sub>5</sub> loading on TiO<sub>2</sub> were prepared. After impregnation process in a rotary evaporator, catalysts were dried and then calcined at 673 K or 773 K for 4 h in air.

**SCR activity measurement of VO<sub>x</sub> in zeolitic microporous TiO<sub>2</sub>.** SCR activity was measured in a fixed-bed quartz tubular reactor. Catalysts were sieved to 300–500 μm in diameter then loaded in the reactor. 500 ppm NO, 500 ppm NH<sub>3</sub>, 2% O<sub>2</sub> and balanced with N<sub>2</sub> were introduced as reactants. In order to examine the catalytic activity in the presence of water, the reactant containing 500 ppm NO, 500 ppm NH<sub>3</sub>, 2% O<sub>2</sub>, 3% H<sub>2</sub>O balanced with N<sub>2</sub> was used. The catalyst was further aged in the presence of 10% O<sub>2</sub>, 5% H<sub>2</sub>O balanced with N<sub>2</sub> at 500 °C for 12 h before catalytic reaction.

Space velocity of inlet gas was maintained to be 40,000 h<sup>-1</sup>. We raised reaction temperature from 423 K to 673 K by 50 K. NO<sub>x</sub> concentration of outlet gas by using NO<sub>x</sub> chemiluminescence analyzer (Model 42i High level, Thermo Scientific). Also, Fourier Transform Infrared (FT-IR) spectroscopy was applied to observe the N<sub>2</sub>O concentration in the gas. We used the average data of 16 scans at a resolution of 1.0 cm<sup>-1</sup>. A Nicolet 6700 (Thermo Scientific) with 2 m gas analysis cell heated to 120 °C to exclude the effect of H<sub>2</sub>O, was used for gas phase analysis.

## References

1. Arakawa, H. *et al.* Catalysis research of relevance to carbon management: Progress, challenges, and opportunities. *Chem. Rev.* **101**, 953–996, doi: 10.1021/Cr000018s (2001).
2. Marten, A. L. & Newbold, S. C. Estimating the social cost of Non-CO<sub>2</sub> GHG emissions: Methane and nitrous oxide. *Energ. Policy* **51**, 957–972, doi: 10.1016/j.enpol.2012.09.073 (2012).
3. Lambert, C. *et al.* Nitrous oxide emissions from a medium-duty diesel truck exhaust system. *Inter. J. Powertrains* **3**, 4–25 (2014).
4. Wallington, T. J., Sullivan, J. L. & Hurlley, M. D. Emissions of CO<sub>2</sub>, CO, NO<sub>x</sub>, HC, PM, HFC-134a, N<sub>2</sub>O and CH<sub>4</sub> from the global light duty vehicle fleet. *Meteorol. Z.* **17**, 109–116, doi: 10.1127/0941-2948/2008/0275 (2008).
5. Gabriëlsson, P. L. T. Urea-SCR in automotive applications. *Top. Catal.* **28**, 177–184, doi: 10.1023/B:Toca.0000024348.34477.4c (2004).
6. Narula, C. K., Daw, C. S., Hoard, J. W. & Hammer, T. Materials issues related to catalysts for treatment of diesel exhaust. *Int J Appl Ceram Tec* **2**, 452–466, doi: 10.1111/j.1744-7402.2005.02046.x (2005).
7. Nova, I., Ciardelli, C., Tronconi, E., Chatterjee, D. & Weibel, M. NH<sub>3</sub>-NO/NO<sub>2</sub> SCR for diesel exhausts after treatment: mechanism and modelling of a catalytic converter. *Top. Catal.* **42–43**, 43–46, doi: 10.1007/s11244-007-0148-4 (2007).
8. Twigg, M. V. Catalytic control of emissions from cars. *Catal. Today* **163**, 33–41, doi: 10.1016/j.cattod.2010.12.044 (2011).
9. Peng, Y., Li, K. H. & Li, J. H. Identification of the active sites on CeO<sub>2</sub>-WO<sub>3</sub> catalysts for SCR of NO<sub>x</sub> with NH<sub>3</sub>: An *in situ* IR and Raman spectroscopy study. *Appl. Catal. B: Environ.* **140**, 483–492, doi: 10.1016/j.apcatb.2013.04.043 (2013).
10. Tian, X., Xiao, Y., Zhou, P., Zhang, W. & Luo, X. Investigation on performance of V<sub>2</sub>O<sub>5</sub>-WO<sub>3</sub>-TiO<sub>2</sub>-cordierite catalyst modified with Cu, Mn and Ce for urea-SCR of NO. *Mater. Res. Innov.* **18**, 202–206, doi: 10.1179/1432891714z.000000000407 (2014).
11. Chen, T., Lin, H., Cao, Q. H. & Huang, Z. Solution combustion synthesis of Ti<sub>0.75</sub>Ce<sub>0.15</sub>Cu<sub>0.05</sub>W<sub>0.05</sub>O<sub>2</sub>-delta for low temperature selective catalytic reduction of NO. *RSC Advances* **4**, 63909–63916, doi: 10.1039/C4ra05862c (2014).
12. Shan, W. P., Liu, F. D., He, H., Shi, X. Y. & Zhang, C. B. A superior Ce-W-Ti mixed oxide catalyst for the selective catalytic reduction of NO<sub>x</sub> with NH<sub>3</sub>. *Appl. Catal. B: Environ.* **115**, 100–106, doi: 10.1016/j.apcatb.2011.12.019 (2012).
13. Wang, Z. H. *et al.* Synergetic Promotional Effects Between Cerium Oxides and Manganese Oxides for NH<sub>3</sub>-Selective Catalyst Reduction Over Ce-Mn/TiO<sub>2</sub>. *Mater. Express* **1**, 167–175, doi: 10.1166/mex.2011.1017 (2011).
14. Chen, L. *et al.* CeO<sub>2</sub>-WO<sub>3</sub> Mixed Oxides for the Selective Catalytic Reduction of NO<sub>x</sub> by NH<sub>3</sub> Over a Wide Temperature Range. *Catal. Lett.* **141**, 1859–1864, doi: 10.1007/s10562-011-0701-4 (2011).
15. Chen, M. J. *et al.* TiO<sub>2</sub> interpenetrating networks decorated with SnO<sub>2</sub> nanocrystals: enhanced activity of selective catalytic reduction of NO with NH<sub>3</sub>. *J. Mater. Chem. A* **3**, 1405–1409, doi: 10.1039/C4ta05503a (2015).
16. Kasuga, T., Hiramatsu, M., Hoson, A., Sekino, T. & Niihara, K. Formation of titanium oxide nanotube. *Langmuir* **14**, 3160–3163, doi: 10.1021/La9713816 (1998).
17. Bavykin, D. V., Parmon, V. N., Lapkin, A. A. & Walsh, F. C. The effect of hydrothermal conditions on the mesoporous structure of TiO<sub>2</sub> nanotubes. *J. Mater. Chem.* **14**, 3370–3377, doi: 10.1039/B406378c (2004).
18. Chi, B., Victorio, E. S. & Jin, T. Synthesis of TiO<sub>2</sub>-based nanotube on Ti substrate by hydrothermal treatment. *J. Nanosci. Nanotechnol.* **7**, 668–672, doi: 10.1166/jnn.2007.147 (2007).
19. Sun, M. H. *et al.* Preparation and Characterization of Pt Nanoparticles Inside Nanotubule TiO<sub>2</sub>. *J. Nanosci. Nanotechnol.* **10**, 3635–3638, doi: 10.1166/jnn.2010.2291 (2010).

20. Cho, J. M., Sun, M. H., Kim, T. H. & Cho, S. J. Formation of Nanotubule, Nanorod and Polycrystalline Nanoparticles TiO<sub>2</sub> by Alkaline Hydrothermal Transformation of Anatase TiO<sub>2</sub>. *J. Nanosci. Nanotechnol.* **10**, 3336–3340, doi: 10.1166/jnn.2010.2293 (2010).
21. Ju, K. Y. *et al.* Enhanced Efficiency of Dye-Sensitized Solar Cells with Novel Synthesized TiO<sub>2</sub>. *J. Nanosci. Nanotechnol.* **10**, 3623–3627, doi: 10.1166/jnn.2010.2277 (2010).
22. Morgado, E. *et al.* A study on the structure and thermal stability of titanate nanotubes as a function of sodium content. *Solid State Sci.* **8**, 888–900, doi: 10.1016/j.solidstatesciences.2006.02.039 (2006).
23. Bavykin, D. V., Kulak, A. N. & Walsh, F. C. Metastable Nature of Titanate Nanotubes in an Alkaline Environment. *Cryst. Growth Des.* **10**, 4421–4427, doi: 10.1021/Cg100529y (2010).
24. Kasuga, T., Hiramatsu, M., Hoson, A., Sekino, T. & Niihara, K. Titania nanotubes prepared by chemical processing. *Adv. Mater.* **11**, 1307–+, doi: 10.1002/(Sici)1521-4095(199910)11:15<1307::Aid-Adma1307>3.3.Co;2-8 (1999).
25. Fehse, M., Monconduit, L., Fischer, F., Tessier, C. & Stievano, L. Study of the insertion mechanism of lithium into anatase by operando X-ray diffraction and absorption spectroscopy. *Solid State Ionics* **268**, 252–255, doi: 10.1016/j.ssi.2014.09.018 (2014).
26. Fehse, M. *et al.* New Insights on the Reversible Lithiation Mechanism of TiO<sub>2</sub> by Operando X-ray Absorption Spectroscopy and X-ray Diffraction Assisted by First-Principles Calculations. *J. Phys. Chem. C* **118**, 27210–27218 doi: 10.1021/Jp507574e (2014).
27. Kwak, J. H., Tran, D., Szanyi, J., Peden, C. H. F. & Lee, J. H. The Effect of Copper Loading on the Selective Catalytic Reduction of Nitric Oxide by Ammonia Over Cu-SSZ-13. *Catal. Lett.* **142**, 295–301, doi: 10.1007/s10562-012-0771-y (2012).
28. Cheng, Y. S. *et al.* The different impacts of SO<sub>2</sub> and SO<sub>3</sub> on Cu/zeolite SCR catalysts. *Catal. Today* **151**, 266–270, doi: 10.1016/j.cattod.2010.01.013 (2010).
29. Herrera, J. E., Kwak, J. H., Hu, J. Z., Wang, Y. & Peden, C. H. F. Synthesis of nanodispersed oxides of vanadium, titanium, molybdenum, and tungsten on mesoporous silica using atomic layer deposition. *Top. Catal.* **39**, 245–255, doi: 10.1007/s11244-006-0063-0 (2006).
30. Kwak, J. H., Herrera, J. E., Hu, J. Z., Wang, Y. & Peden, C. H. F. A new class of highly dispersed VO<sub>x</sub> catalysts on mesoporous silica: Synthesis, characterization, and catalytic activity in the partial oxidation of ethanol. *Appl. Catal. A: Gen.* **300**, 109–119, doi: 10.1016/j.apcata.2005.10.059 (2006).
31. Madia, G., Elsener, M., Koebel, M., Raimondi, F. & Wokaun, A. Thermal stability of vanadia-tungsta-titania catalysts in the SCR process. *Appl. Catal. B: Environ.* **39**, 181–190, doi: Pii S0926-3373(02)00099-1, doi: 10.1016/S0926-3373(02)00099-1 (2002).
32. Yates, M., Martin, J. A., Martin-Luengo, M. A., Suarez, S. & Blanco, J. N<sub>2</sub>O formation in the ammonia oxidation and in the SCR process with V<sub>2</sub>O<sub>5</sub>-WO<sub>3</sub> catalysts. *Catal. Today* **107-08**, 120–125, doi: 10.1016/j.cattod.2005.07.015 (2005).

## Acknowledgements

This project is supported by the “R&D Center for reduction of Non-CO<sub>2</sub> Greenhouse gases (0458-20140019)” funded by Korea Ministry of Environment(MOE) as “Global Top Environment R&D Program”. Funders have no role in study design, data collection and analysis, decision to publish, or preparation of the manuscript.

## Author Contributions

S.G.L. and H.J.L. synthesized the zeolitic microporous TiO<sub>2</sub> and performed the samples characterization and data analysis. I.S. and S.Y. performed the catalytic experiments investigation. D.H.K. and S.J.C. designed the research. All authors co-wrote the manuscript.

## Additional Information

**Competing financial interests:** The authors declare no competing financial interests.

**How to cite this article:** Lee, S. G. *et al.* Suppressed N<sub>2</sub>O formation during NH<sub>3</sub> selective catalytic reduction using vanadium on zeolitic microporous TiO<sub>2</sub>. *Sci. Rep.* **5**, 12702; doi: 10.1038/srep12702 (2015).



This work is licensed under a Creative Commons Attribution 4.0 International License. The images or other third party material in this article are included in the article’s Creative Commons license, unless indicated otherwise in the credit line; if the material is not included under the Creative Commons license, users will need to obtain permission from the license holder to reproduce the material. To view a copy of this license, visit <http://creativecommons.org/licenses/by/4.0/>